


Empirical Distance Metrics Relationships and Uncertainties in Seismic Hazard Assessment

Melish Kayastha¹, Shahram Pezeshk^{*1} , and Behrooz Tavakoli²

ABSTRACT

The seismic hazard of an area is determined based on the ground motion observed at that site. The intensity of the ground motion can be predicted using ground-motion models (GMMs). GMMs typically use distance metrics such as the Joyner–Boore distance (R_{JB}) and the rupture distance (R_{RUP}). However, apart from R_{JB} and R_{RUP} , probabilistic seismic hazard analysis (PSHA) also utilizes point-source-based distances like the epicentral distance (R_{EPI}) and the hypocentral distance (R_{HYP}). These distance metrics are used for point sources when the fault geometry is unknown or is ignored. To obtain an accurate seismic hazard of an area, we need to determine the relationship between the distance metrics. In this study, we develop empirical relationships between R_{JB} and various other distance metrics. This method avoids conducting computationally intensive tasks such as computing finite-fault-based distances for different fault geometry of a virtual rupture plane for each point source. The empirical equations provide the relation between R_{JB} and target distance metric (R_{target}) based on the magnitude of the earthquake and the dip angle of the fault. In addition, we also require the depth to the top of the rupture to calculate R_{HYP} . We discuss the steps to include the variability due to the conversion of the distance metrics in the PSHA. We have compared the results of this study with other published studies for distance conversion. A simple PSHA study of a circular area of 100 km using Pezeshk *et al.* (2011) as the GMM determined an increase in hazard using the proposed empirical equations and their uncertainties. The equations developed in this study can be directly applied in PSHA and are independent of the GMMs used for seismic hazard calculations. The equations can also be used for different fault geometries with a range of dip angles varying from 10° to 90°, for magnitudes 5.0–8.0, and distances up to 200 km. We have focused on the central and eastern United States.

KEY POINTS


- Probabilistic seismic hazard analysis (PSHA) must use consistent distance metrics throughout the analysis to obtain accurate seismic hazards.
- The empirical equations provide the relation between two distance metrics based on the magnitude and dip angle.
- These equations are independent of the ground-motion models (GMMs) and can be directly used in PSHA.

[Supplemental Material](#)

INTRODUCTION

Researchers use different distance metrics to determine the source-to-site distance measure during an earthquake. The most used distance metrics are the Joyner–Boore distance (R_{JB}), the rupture distance (R_{RUP}), the epicentral distance (R_{EPI}), and the hypocentral distance (R_{HYP}). R_{JB} measures the closest distance to the surface projection of the fault; R_{RUP} measures the closest distance to the ruptured fault; R_{EPI} measures the distance to the

epicenter of an earthquake; and R_{HYP} measures the distance to the hypocenter of an earthquake. R_{JB} and R_{RUP} are classified as fault-based distances, whereas R_{EPI} and R_{HYP} are classified as point-based distances. Many researchers have used point-based distance metrics to develop their GMMs. However, there were issues with large magnitudes at close distances for such models resulting in unreliable seismic hazard calculations. Hence, GMMs usually use either R_{JB} or R_{RUP} to determine the ground motions in an area. However, the seismicity of some areas cannot be associated with known faults. In such cases, probabilistic seismic hazard analysis (PSHA) uses point-source models to describe the seismic hazard because such models can be used for gridded seismicity (Tavakoli *et al.*, 2018). Hence, it may

1. Department of Civil Engineering, The University of Memphis, Memphis, Tennessee, U.S.A.,  <https://orcid.org/0000-0002-4367-1184> (SP); 2. Department of Seismology and Geophysics, G&HES, Bechtel Power Corporation, San Francisco, California, U.S.A.

*Corresponding author: mkyastha@memphis.edu

Cite this article as Kayastha, M., S. Pezeshk, and B. Tavakoli (2023). Empirical Distance Metrics Relationships and Uncertainties in Seismic Hazard Assessment, *Bull. Seismol. Soc. Am.* **XX**, 1–16, doi: [10.1785/0120220193](https://doi.org/10.1785/0120220193)

© Seismological Society of America

be necessary to convert from one distance metric to another to accurately determine an area's seismic hazard in conducting PSHA. Monelli *et al.* (2014) found differences of as much as 54% in a PSHA sensitivity study when using point-based and fault-based distances, which resulted in a considerable underestimation of the hazard, especially for large earthquakes. Tavakoli *et al.* (2018) also demonstrated that effective R_{EPI} distance developed higher seismic hazards than R_{JB} distance. There are a few methods to avoid this problem. We have discussed three approaches subsequently.

APPROACH 1

One approach would be to convert from one distance metric to another. Scherbaum *et al.* (2004) used R_{JB} as the primary distance metric to obtain R_{EPI} , R_{HYP} , R_{RUP} , and the distance to the seismogenic part of the rupture plane. They simulated various earthquake events based on the magnitude, dip angle, and location of the hypocenter on the fault. The simulation was conducted for different cases: strike-slip, dip-slip, and a general case in which the style of faulting is unknown. A residual function based on the gamma distribution was used to describe other distance metrics based on R_{JB} . The residual function, the difference between the target distance metric and reference distance metric (R_{JB}), is always positive because the R_{JB} distance is always smaller than or equal to other target distance metrics. The polynomial functions are applicable for shallow intercontinental earthquake events for R_{JB} distances from 0 to 100 km and moment magnitudes between 5.0 and 7.5. They also provided coefficients to calculate the standard deviation.

Electric Power Research Institute (EPRI, 2004) developed empirical relationships between R_{EPI} , R_{JB} , and R_{RUP} for the central and eastern United States (CEUS). The ruptured area (RA) was determined using the Somerville *et al.* (2001) relation. The length-to-width aspect ratio of 3 for the strike-slip fault and 2 for the dip-slip fault were used. A dip angle of 40° was assumed for the dip-slip fault. EPRI (2004) also constrained the maximum depth to 25 km. R_{EPI} was chosen as the primary distance metric to obtain R_{JB} and R_{RUP} . EPRI (2004) developed four ground-motion models (GMMs) for the CEUS and provided distance conversion relations for each GMM. EPRI (2004) also provided equations to calculate the additional aleatory variability to determine the total variability in PSHA for each GMM.

APPROACH 2

As another approach, Bommer and Akkar (2012) suggested that two different sets of coefficients for point-source-based models and finite-source-based models should be developed for GMMs. However, few researchers have provided coefficients for point-source- and finite-source-based distances for their GMMs. Akkar *et al.* (2014) provided the coefficients for both point-based and fault-based distances for their GMM for Europe and the Middle East. Bommer *et al.* (2016) simulated many R_{EPI} and R_{JB} distance combinations based on a range of fault orientations

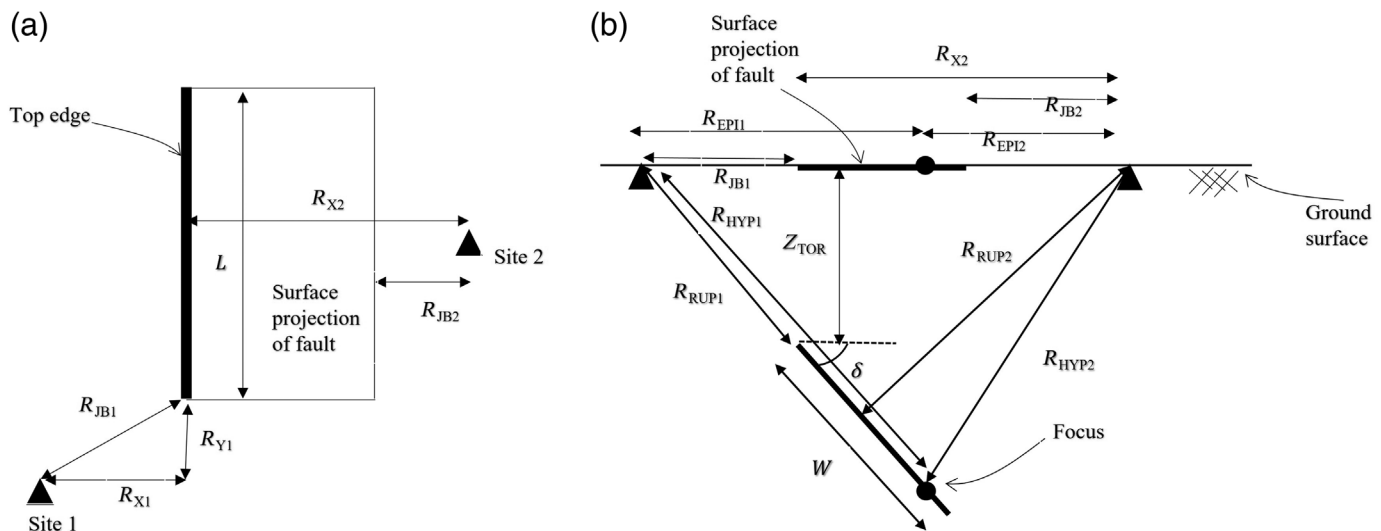
and fault dimensions to determine the variability in their GMMs for induced seismicity. They used Wells and Coppersmith (1994) to determine the rupture length because no appropriate magnitude-scaling relationship was available for induced seismicity. They calculated a range of R_{JB} values for a given R_{EPI} distance and then used Akkar *et al.* (2014) to determine the median values for spectral acceleration. Finally, they calculated the variability due to R_{EPI} and its respective R_{JB} values. They modeled sigma as a Gaussian distribution. This approach can be directly applied without converting the distances by including the sigma in the total GMM variability for PSHA calculations. However, the equation for variability cannot be used for other GMMs.

APPROACH 3

The third approach would be to simulate pseudoruptures for each scenario based on dimensions obtained using different magnitude-scaling relationships such as Wells and Coppersmith (1994), Somerville (2014), or others. Kakkamanos *et al.* (2011) developed the relationship between R_{JB} and R_{RUP} based on the geometrical properties of the fault. For a given dip angle (δ), down-dip rupture width (W), depth to the top of rupture (Z_{TOR}), and R_{JB} , they provided the relation to determine the R_{rup} for different source-to-size azimuth (α). They have also suggested different relationships for δ , W , and Z_{TOR} if these values are unknown. They compared their results to those obtained by Scherbaum *et al.* (2004) and found them slightly different.

Thompson and Worden (2018) derived mean R_{JB} and R_{RUP} constrained on R_{EPI} , magnitude, and azimuth. They also provided adjustment factors for GMM standard deviations to include the uncertainty due to the conversion of different distances. For simulation, they used different distance conversion equations provided in Somerville (2014) for the stable continental region (SCR), Hanks and Bakun (2008) for the active continental region (ACR), and Wells and Coppersmith (1994) for both cases. The length-to-width aspect ratio of 1 for SCR and 1.7 for ACR was assumed. They observed the mean R_{JB} decreased as the dip angle decreased. The ratio of the mean R_{JB} to R_{EPI} varied from 0 at small distances to 1 at larger distances, whereas the ratio of the mean R_{RUP} to R_{EPI} is greater than 1 at smaller distances and approaches 1 at very large distances. The variation of R_{RUP} at small R_{EPI} distance is controlled by the distribution of depth to top of rupture (Z_{TOR}).

Tavakoli *et al.* (2018) proposed an analytical distance conversion method to convert R_{JB} distance to R_{EPI} , R_{HYP} , or R_{RUP} distance based on the geometry of the fault and the distribution of the hypocenter. The distance obtained can be combined with other seismological constraints, such as geometric spreading and attenuation parameters, to obtain effective distances that can demonstrate the effect of extended fault sources at small distances. Effective distances are based on equivalent point-source modeling. In equivalent point-source modeling, the rupture originated from a virtual point at an effective



distance from the site such that there is no saturation effect at close distances. The method developed can be employed for different magnitudes, distances, and site-specific conditions to obtain an accurate conversion between different distance metrics for the specific region. A method to account for the uncertainty has also been discussed. As the method is generic, it can be applied to different cases of earthquake rupture, large, small, or even induced earthquakes.

In current PSHA methodologies for U.S. Geological Survey (USGS), [Petersen et al. \(2010\)](#) assume the seismic energy is released from the epicenter rather than the crust of the ruptured fault. They use R_{EPI} as the reference distance to calculate R_{JB} for a vertical strike-slip fault for different azimuths ranging from 0° to 360° . They assume the epicenter is at the center of the fault, and they used [Wells and Coppersmith \(1994\)](#) for the magnitude-scaling relationship.

The distance conversion equations developed by [EPRI \(2004\)](#) depend on the GMMs and frequency. [Scherbaum et al. \(2004\)](#) do not consider the effect of hanging wall and footwall. [Kaklamanos et al. \(2011\)](#) do not include a conversion method between point-source distance metrics and extended fault distance metrics. Calculating seismic hazard is a computationally intensive process. The method developed by [Thompson and Worden \(2018\)](#) and [Tavakoli et al. \(2018\)](#), which involves integration at different possible virtual faults or virtual sites, may not be practical for large data sets. In addition, the current USGS approach is only practical for vertical strike-slip fault and may not be suitable for dip-slip faults. In this study, we develop simple empirical relationships between R_{JB} and target distance metrics ($R_{target} = R_{RUP}, R_{EPI}, R_{HYP}$), which are independent of GMMs. We also consider the effect of hanging wall and footwall.

ESTIMATION OF DISTANCE METRICS PARAMETERS

Figure 1 shows the different distance metrics discussed in this study. The equations to determine R_{RUP} based on the geometry

Figure 1. (a) Illustration of the plan view of the fault. The rectangle is the surface projection of the fault, with the bold line as the surface projection of the top edge of the fault. The triangles are locations of possible sites or stations with their respective distance metrics. Site 1 is located at the footwall of the fault and has a negative value for R_X , whereas site 2 is located at the hanging-wall side of the fault and has a positive R_X value. R_Y is 0 for site 2. (b) Illustration of the vertical cross section of a fault. Also shown are various distance metrics R_X , Joyner–Boore distance (R_{JB}), rupture distance (R_{RUP}), epicentral distance (R_{EPI}), and hypocentral distance (R_{HYP}) measured from the site (shown by a triangle) to the fault.

of the fault are derived from [Kaklamanos et al. \(2011\)](#). Similarly, we have used equations for R_{EPI} and R_{HYP} provided by [Tavakoli et al. \(2018\)](#). Apart from R_{RUP} , R_{EPI} , and R_{HYP} , we still need additional distance metrics, such as R_X and R_Y , which facilitate the conversion from R_{JB} to the target distance measure. The equations to determine these distances are discussed in this section.

R_X is the closest perpendicular distance from the site to the projection of the top edge of the ruptured fault. Beyond the limits of the strike of the fault, it is calculated perpendicular to the extension of the projection of the top edge of the fault along the strike. This distance metric is used in GMMs such as [Abrahamson and Silva \(2008\)](#), [Chiou and Youngs \(2008\)](#), and [Campbell and Bozorgnia \(2014\)](#) to quantify hanging-wall effects. Unlike other distance metrics, which always have positive values, R_X can be positive or negative—positive for sites on the hanging-wall side of the fault and negative for sites on the footwall side of the fault ([Kaklamanos et al., 2011](#)). Table 1 provides the equations for R_X developed in this study for different cases based on the azimuth angle (θ), which is the angle from the center of the fault to the site.

R_Y is the closest parallel distance from the site to the projection of the ruptured fault. The equations to calculate R_Y developed in this study are presented in equation (1). R_{cRef} is the epicentral distance calculated from the center of the fault. The equations for terms such as R_{cRef} , θ_0 , θ_1 , and the derivations

TABLE 1

Equation to Calculate R_X Based on Joyner–Boore Distance (R_{JB}), Length (L), and Width (W) of the Fault, Dip Angle (δ), and Azimuth Angle (θ)

Azimuth Angle	Case	Equation
$\theta \in (0, \frac{\pi}{2})$	$0 \leq \theta < \theta_1$	$0.5W \cos(\delta) + \tan(\theta) (0.5L + R_{JB})$
$\theta \in (-\frac{\pi}{2}, 0)$		$0.5W \cos(\delta) - \tan(\theta) (0.5L + R_{JB})$
$\theta \in (0, \frac{\pi}{2})$	$\theta_1 \leq \theta < \theta_0$	$0.5W \cos(\delta) + R_{cRef} \sin(\theta)$
$\theta \in (-\frac{\pi}{2}, 0)$		$-0.5W \cos(\delta) + R_{cRef} \sin(\theta)$
$\theta \in (0, \frac{\pi}{2})$	$ \theta \geq \theta_0$	$W \cos(\delta) + R_{JB}$
$\theta \in (-\frac{\pi}{2}, 0)$		R_{JB}

for R_X and R_Y have been provided in the supplemental material, available to this article

$$R_Y = \begin{cases} 0 & |\theta| \geq \theta_0 \\ R_{cRef} \cos(|\theta|) - 0.5L & \theta_1 \leq |\theta| < \theta_0 \\ R_{JB} & |\theta| < \theta_1 \end{cases} \quad (1)$$

The mean R_{EPI} distance (Tavakoli *et al.*, 2018) can be determined for a given R_{JB} , δ , and magnitude as follows:

$$E[R_{EPI}|R_{JB}, M_w, \delta] = \int_{-3}^3 \int_0^{2\pi} \int_0^{W \cos(\delta)} \int_{-0.5L}^{0.5L} R_{EPI}(x, y, \theta, \epsilon) p(x) p(y) p(\theta) p(\epsilon) dx dy d\theta d\epsilon, \quad (2)$$

in which $R_{EPI}(x, y, \theta, \epsilon)$ is the distance from the epicenter (x, y) of the fault to the site located at an azimuth angle (θ) from the fault. “ ϵ ” is used to incorporate the uncertainties in the scaling relationship used to determine “ L ” and “ W ” from the magnitude of the fault. We have used ± 3 standard deviations, assuming a standard normal distribution for our calculation.

Using this equation, we can obtain R_{EPI} from the fault to the site at different R_{JB} and θ . For the calculation, we determine the mean value of R_{EPI} at all possible $\theta \in (0^\circ, 360^\circ)$ for a given R_{JB} distance, magnitude, and dip angle. “ x ” and “ y ” are the variables along the length and the width of the fault. We can use different distribution functions to define the spacing that can describe the characteristics of the fault rupture. We have used Mai *et al.* (2005) for our calculations to determine the hypocenter distribution along the strike and down-dip direction. After integration along the length and width of the fault, all possible locations of the epicenter can be considered. Instead of defining a complex function to express the distribution of θ , we used a small spacing for θ , which also provided results with acceptable accuracy without hampering the computational efficiency (Campbell and Gupta, 2018). For our calculation, we have used a spacing of 1° with uniform distribution ($P(\theta) = 1/2\pi$). For “ ϵ ”, we used a spacing of 1.0. We have calculated the mean values at different dip angles from 10° to 90° with a spacing of 10° .

The mean R_{HYP} distance (Tavakoli *et al.*, 2018) can be calculated as follows:

$$E[R_{HYP}|R_{JB}, M, \delta] = \int_{-3}^3 \int_0^{2\pi} \int_{Z_{TOR}}^{Z_{TOR} + W \sin(\delta)} \int_0^{W \cos(\delta)} R_{HYP}(x, y, z, \theta, \epsilon) p(x) p(y) p(z) p(\theta) p(\epsilon) dx dy dz d\theta d\epsilon. \quad (3)$$

In addition to all the parameters specified in equation (2), we also have the depth term “ z ”, which varies from the depth to the bottom of the rupture ($Z_{TOR} + W \sin(\delta)$) to the depth to the top of the rupture (Z_{TOR}). The hypocentral depth is determined by Scherbaum *et al.* (2004).

The mean R_{RUP} (Tavakoli *et al.*, 2018) can be calculated as follows:

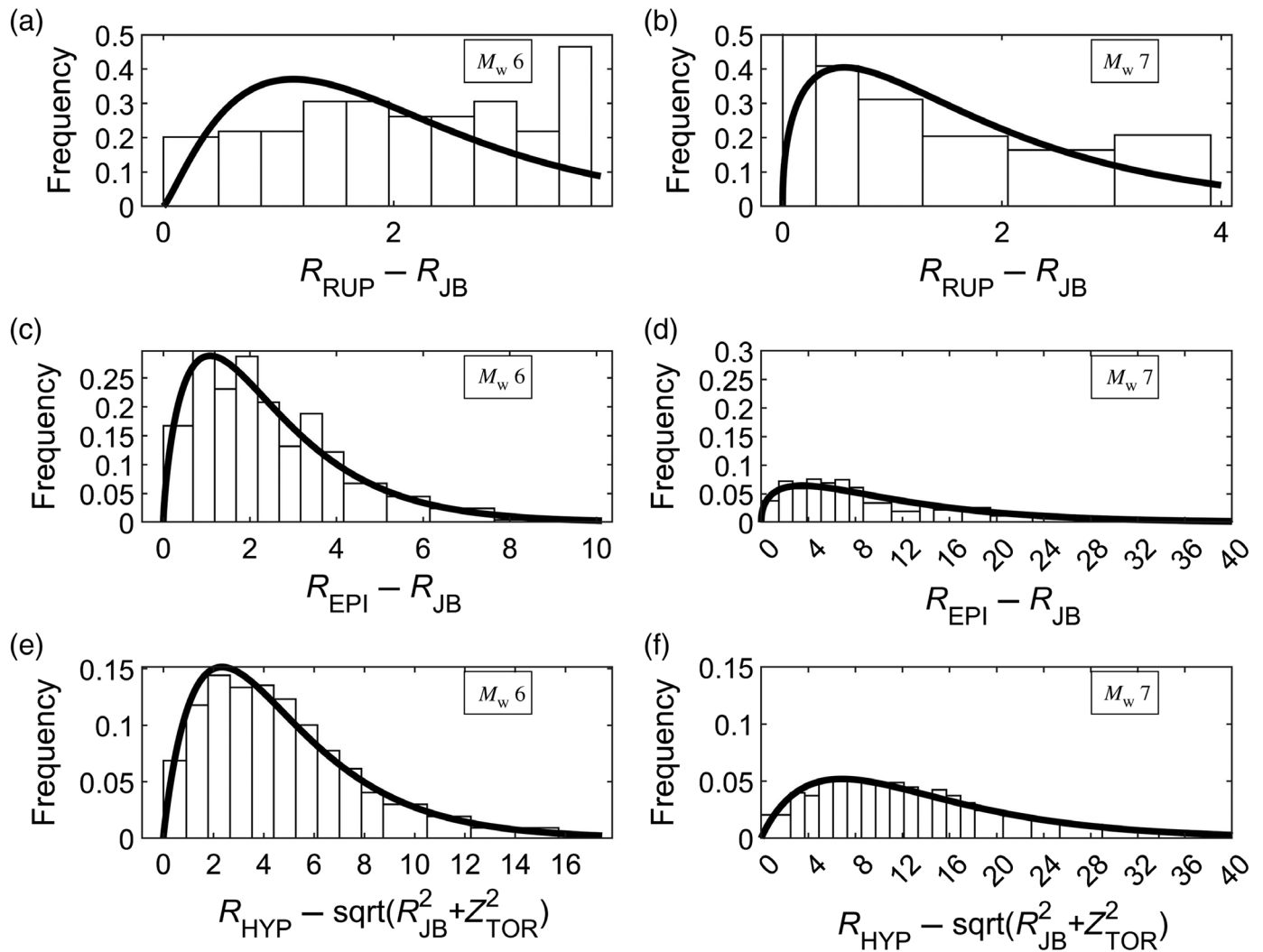
$$E[R_{RUP}|R_{JB}, M, \delta] = \int_{-3}^3 \int_0^{2\pi} R_{RUP}(\theta, \epsilon) p(\theta) p(\epsilon) d\theta d\epsilon. \quad (4)$$

Because R_{RUP} is a fault-based distance metric, we do not need to discretize the fault. Instead, we calculate R_{RUP} values at different azimuths for a given R_{JB} , dip angle, and magnitude. The parameters have been defined previously.

FAULT MODEL ASSUMPTIONS

The data for this study are developed based on the centroid-centered virtual site model (Tavakoli *et al.*, 2018; Campbell and Gupta, 2018). In this approach, the fault is fixed, and the virtual site moves around the fault. The location of the azimuth is dependent on the azimuth of the site from the centroid of the ruptured fault. The virtual sites are located at a constant R_{JB} distance from the fault. For a constant R_{JB} distance, a range of values for other distance metrics (R_{RUP} , R_{EPI} , and R_{HYP}) can be obtained based on the magnitude, dip angle, and azimuth of the fault. R_{JB} is chosen as the reference distance because there is only one possible station for a known fault at a given azimuth. For R_{EPI} , the location of the station at a given azimuth can vary based on the location of the epicenter at fault. The mean value of the reference distance metric is obtained to develop the statistical relationship between the different distance metrics. For computational efficiency, instead of solving for the integral, we have discretized the fault along the length, width, and depth of the fault, and an azimuth increment of 1° for the virtual site. The length and width are discretized such that the reference sites are densely spaced closer to the fault and sparsely spaced away from the fault.

Different fault ruptures have been considered based on the size of the rupture, the geometry of the rupture plane, and the location of the hypocenter. The geometry of the rupture plane is modeled as a rectangular plane with length (L), width (W), dip angle (δ), and depth to the top of the rupture (Z_{TOR}), as shown in Figure 1. The size of the rupture, based on magnitude, is used to model the length and width of the fault. We have focused on the CEUS region. So, we used the equation



provided in [Somerville \(2014\)](#), developed for the CEUS region, to calculate the RA of the rupture plane for different magnitudes. We use a fixed length-to-width aspect ratio of 1. The hypocentral depth values are based on [Scherbaum et al. \(2004\)](#). If the calculated rupture plane is extended above the surface, the width of the fault is adjusted such that the top of the fault lies on the surface. The width is restricted to the seismogenic zone (15 km, [Shaw and Wesnousky, 2008](#)). Modification of Z_{TOR} also changes the dimensions for the width of the fault (assuming a fixed hypocentral depth). Consequently, the length is increased to maintain a constant RA for a given M . The data are generated for M values between 5 and 8, dip angles from 10° to 90° and R_{JB} values up to 200 km. The azimuth value is varied from 0° to 360° . We determine the target distances, such as R_{EPI} , R_{HYP} , and R_{RUP} , for each geometrical scenario using the equations discussed previously.

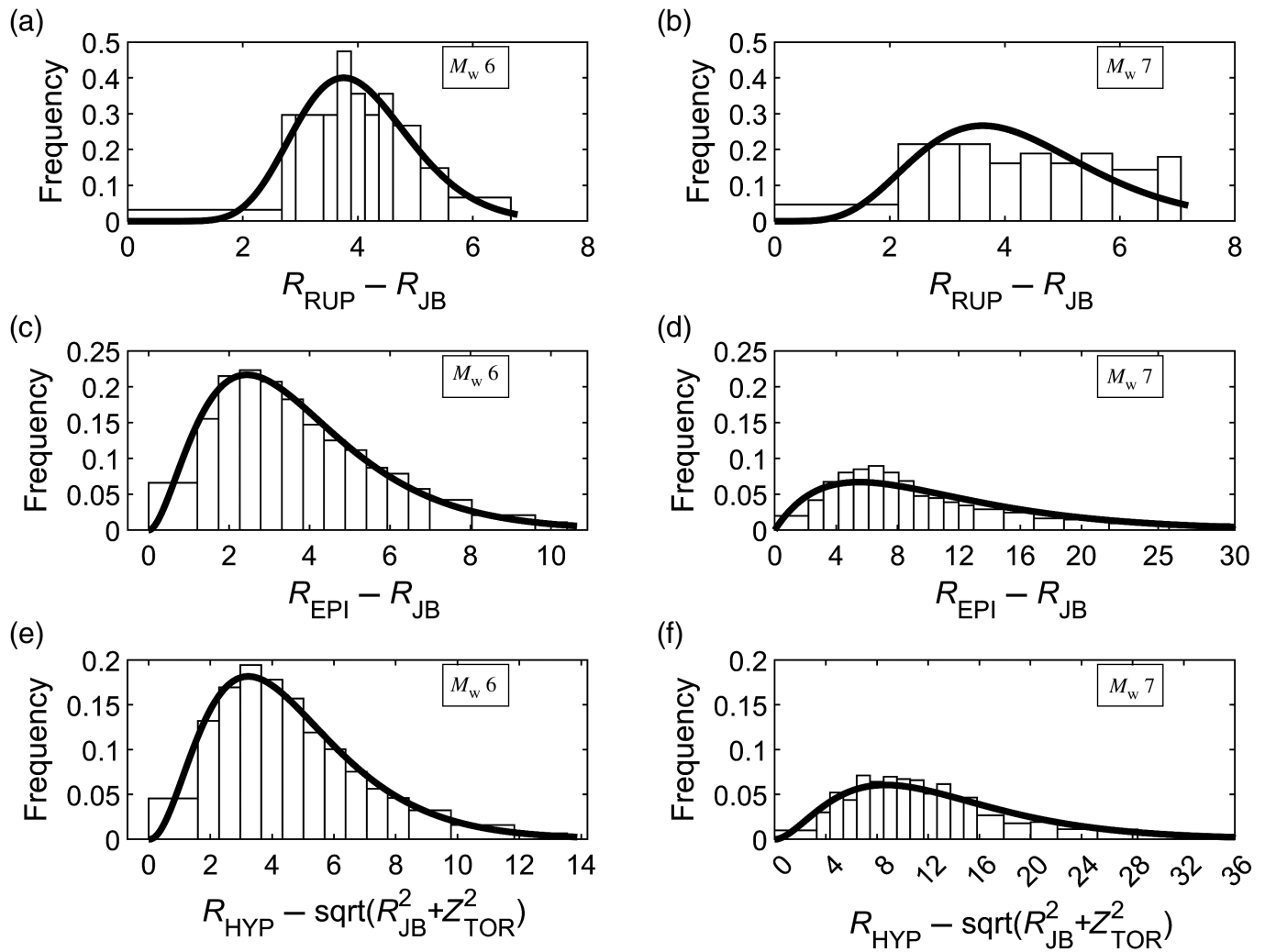
This approach provides us with a range of target distance values for a given R_{JB} value. The target distances depend on R_{JB} , length (L), width (W), and dip (δ) of the rupture plane, the azimuth angle (α), the hypocentral depth, depth to the top of the rupture (Z_{TOR}), and the style of faulting (strike-slip

Figure 2. Histogram plots of the difference for (a,b) R_{RUP} , (c,d) R_{EPI} , and (e, f) R_{HYP} for a vertical strike-slip fault at (a,c,e) magnitude 6 and (b,d,f) magnitude 7 at an R_{JB} of 10 km. The solid line represents the gamma distribution fitted to the histogram. The mean and the standard deviation of the distribution are used in regression analysis to determine the coefficients at different M , R_{JB} , and dip angle (δ) in the empirical equations for R_{EPI} , R_{RUP} , and R_{HYP} .

or dip-slip). Regression analysis based on the nonlinear least-squares method is performed on the obtained data to develop empirical relations for R_{RUP} and R_{EPI} based on the R_{JB} , magnitude of the fault and dip angle, and R_{HYP} based on R_{JB} , M , δ , and Z_{TOR} .

EMPIRICAL MODELS FOR DISTANCE METRICS CONVERSION

Figures 2 and 3 show the histogram plots for the difference between R_{target} and R_{JB} at $M_w 6$ (panels a,c,e) and $M_w 7$ panels b,d,f) at R_{JB} of 10 km for vertical strike-slip fault and 40° dip-slip fault, respectively. The difference can be modeled as a gamma distribution (shown as the solid line) to determine



the mean and the standard deviation of the target distance metric. For $M_w 6$, the range of distributed values is small, varying from 0 to 3 km for R_{RUP} , 0 to 10 km for R_{EPI} , and 0 to 16 km for R_{HYP} for vertical strike-slip fault. The range of distributed values increases for $M_w 7$, varying from 0 to 4 km for R_{RUP} , 0 to 40 km for R_{EPI} , and 0 to 40 km for R_{HYP} for vertical strike-slip fault. Similar distributions can be developed for each target distance metric at different R_{JB} , M , and δ . We conducted a non-linear least-squares regression analysis for the data to develop a suitable empirical relation between R_{JB} and the target distance. For regression, we used the mean value of the target distances at different azimuths for a given R_{JB} distance. To determine the correlation between the target distance metric and R_{JB} , we choose an appropriate functional form that best describes their relationship. The functional form is dependent on the M , Z_{TOR} , and δ of the fault and can be presented as

$$R_{target} = f(R_{JB}, M, \delta, Z_{TOR}) + \sigma, \quad (5)$$

in which σ is the sigma, which measures the standard deviation due to variation in different parameters such as the location of

Figure 3. Histogram plots of the difference for (a,b) R_{RUP} , (c,d) R_{EPI} , and (e, f) R_{HYP} for a 40° dip-slip fault at (a,c,e) magnitude 6 and (b,d,f) magnitude 7 at an R_{JB} of 10 km. The solid line represents the gamma distribution fitted to the histogram. The mean and the standard deviation of the distribution are used in regression analysis to determine the coefficients at different M , R_{JB} , and δ in the empirical equations for R_{EPI} , R_{RUP} , and R_{HYP} .

the hypocenter, azimuth, and geometry of the fault. Separate equations have been presented for dip-slip fault and vertical strike-slip fault. For the vertical strike-slip fault, the width of the fault does not impact the calculation of the target distance, but the width of the fault is an essential parameter for the dip-slip fault. Because of this, the final values obtained for both cases are different from each other and are better represented if we conduct separate regressions on these data sets. For cases with more information, such as the location of the hypocenter or azimuth, Approach 3 discussed earlier would provide better results than the proposed empirical equations. The proposed empirical equations would only provide mean values considering random azimuth and hypocenter locations.

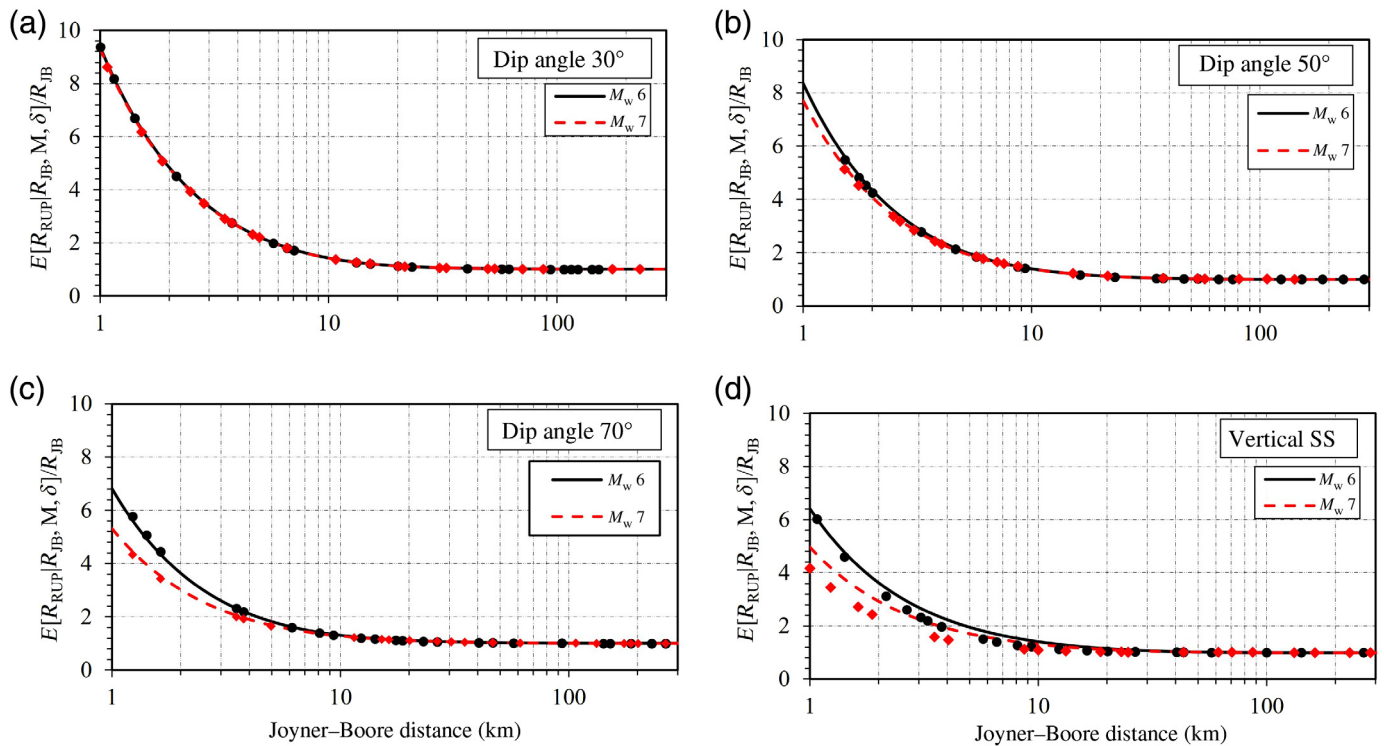


Figure 4. Comparison of the ratio of R_{RUP} to R_{JB} versus R_{JB} for dip-slip fault with dip angles of (a) 30° , (b) 50° , and (c) 70° , and (d) vertical strike-slip fault for moment magnitudes of 6 (solid line) and 7 (dashed line). The dots represent the mean values for the distribution and the lines represent the empirical equations fitted to the distribution. The color version of this figure is available only in the electronic edition.

MEAN MODELS FOR DISTANCE METRICS CONVERSIONS

Joyner–Boore distance and rupture distance

Based on equation (4), we determine the mean R_{RUP} distance for a given R_{JB} distance at different lengths, widths, and the dip of the fault. Because of symmetry, only azimuth angles from -90° to 90° are used for calculation. Separate regression analysis was carried out for vertical strike-slip fault and dip-slip fault. At different dip angles, the coefficients for the dip-slip fault are different. The relationship between R_{JB} and R_{RUP} for dip-slip fault can be represented as

$$E[R_{\text{RUP}}|R_{\text{JB}}, M, \delta] = R_{\text{JB}} + C_1 \exp(-C_2(M - 5)) \exp(-C_3 R_{\text{JB}}) + C_4 \exp(-C_5 R_{\text{JB}}) \pm CF_{\text{HW}} + \sigma_{\text{RUP}},$$

$$CF_{\text{HW}} = C_6 \exp(C_7(M - 5)) \exp(-C_8 R_{\text{JB}}), \quad (6)$$

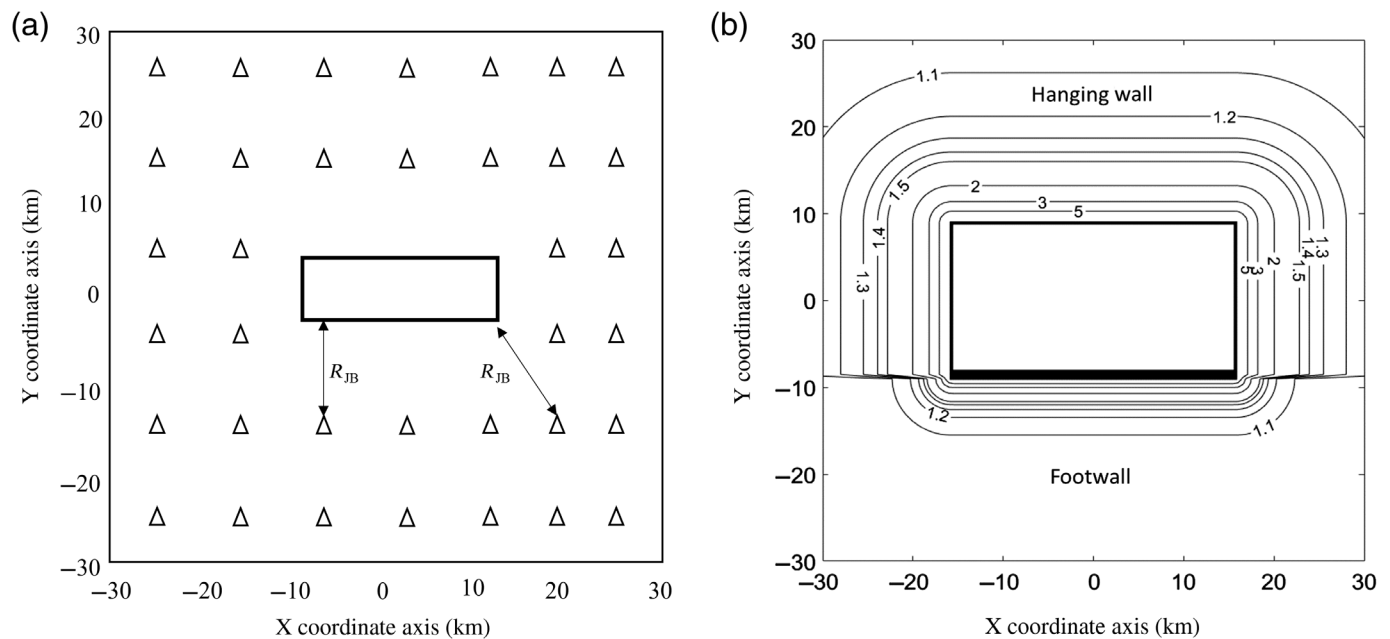
in which parameters C_1 to C_8 are the regression coefficients and CF_{HW} is the hanging-wall and footwall parameter. Coefficients C_1 to C_8 are obtained from regression analysis and are provided in Table 2. The coefficients for dip angles not listed can be determined using interpolation. σ_{RUP} is the standard deviation discussed in the [Sigma Model for Distance Metrics Conversions](#) section.

Similarly, for a vertical strike-slip fault:

$$E[R_{\text{RUP}}|R_{\text{JB}}, M, \delta] = R_{\text{JB}} + C_1 \exp(-C_2(M - 5)^2) \exp(-C_3 R_{\text{JB}}) + C_4 \exp(-C_5 R_{\text{JB}}) + \sigma_{\text{RUP}}. \quad (7)$$

The equations are valid only when $R_{\text{JB}} \sim 0$. When $R_{\text{JB}} = 0$, the mean R_{RUP} is also zero. As shown in Figure 4, the values

obtained from the empirical equation (represented as lines) closely align with the mean data obtained from equation (4) (represented by dots). R_{RUP} is considerably larger than R_{JB} at shorter distances (<10 km), but the values converge at larger R_{JB} distances (>30 km). R_{RUP} varies with the dip angle of the fault and the magnitude of the earthquake event, though the variation is mainly observed below 20 km. At smaller distances, we observe that R_{RUP} decreases as the magnitude increases, though this effect is not observed for smaller dip angles ($\delta = 30^\circ$). For the dip-slip fault, R_{RUP} distance is always measured from the top of the rupture to the site on the footwall side of the fault. However, at the hanging-wall side of the fault, R_{RUP} is also dependent on the depth of the rupture and dip angle. So, R_{RUP} calculated on the footwall side of the fault is always smaller than or equal to R_{RUP} calculated on the hanging-wall side of the fault for a constant R_{JB} distance, as shown in Figure 1b. This effect is represented by the CF_{HW} term, which is positive on the hanging-wall side of the fault and negative on the footwall side of the fault. The effect can be observed in the contour plot for the ratio of R_{RUP} to R_{JB} shown in Figure 5 for a dip-slip fault with a 50° dip angle and M_w 7. We have a 60 km by 60 km plot varying from -30 to 30 in both directions, as shown in Figure 5a. The center of the fault is located at the center of the plot (0,0). We



generate observation sites on the plot with a gridded density of 1 km (only a small sample of observation sites are shown in Fig. 5a for clarity). For each observation point, we calculate R_{JB} and R_{RUP} from the fault. We divide R_{RUP} by R_{JB} to determine the ratio. We then use the calculated ratios to plot the contour map shown in Figure 5b. On the footwall side of the fault, the contours of the ratios are closer together, representing smaller R_{RUP} values for the same R_{JB} values. The contours of the ratios are farther apart at the hanging side of the fault. In addition, R_{RUP} and R_{JB} values are the same (representing the ratio of 1) for R_{JB} greater than 15 km for the footwall and 25 km for the hanging wall. The effect of the footwall and hanging wall is not observed for a vertical strike-slip fault.

Joyner–Boore distance and epicentral distance

The azimuth angles from 0° to 90° can model the entire range of possible values for R_{EPI} for a given R_{JB} distance at a given length,

Figure 5. (a) A 60 km by 60 km plot showing the location of the fault and the observation sites. The triangles represent the observation sites located at every 1 km R_{JB} distance from the center (0,0) (only a small sample of observation sites are shown for clarity). The length and width of the fault are based on the magnitude and dip angle. The center of the fault is (0,0). (b) Contour plot for the ratio of R_{RUP} to R_{JB} for M_w 7 and dip angle 50° . The contour of the ratios is closer together at the footwall side of the fault than the hanging-wall side of the fault because R_{RUP} for a given R_{JB} is smaller at the footwall compared to the hanging-wall side of the fault.

width, and dip angle of the fault. The regression analysis is performed separately for the dip-slip fault ($\delta \neq 90^\circ$) and vertical strike-slip fault ($\delta = 90^\circ$). The functional form that can fit the mean values of R_{EPI} at different R_{JB} for dip-slip fault is

$$E[R_{EPI}|R_{JB}, M, \delta] = R_{JB} + C_1 \exp(C_2(M-5)^2)(R_{JB}^{C_3} - C_4) + C_5 R_{JB}^{C_6} + C_7 \exp(C_8(M-5)) + \sigma_{EPI}. \quad (8)$$

TABLE 2

Coefficients for $E[R_{RUP}|R_{JB}, M, \delta]$ at Different Dip Angles (δ) for a Given Magnitude (M) and Joyner–Boore Distance (R_{JB})

δ	Mean					Footwall			Hanging Wall		
	C_1	C_2	C_3	C_4	C_5	C_6	C_7	C_8	C_6	C_7	C_8
10	2.921	0.0561	0.0193	7.230	0.1330	0.4552	0.4328	0.0378	0.2143	0.6287	0.0309
20	2.791	0.0379	0.0184	7.015	0.1265	0.7921	0.4583	0.0350	0.3910	0.6414	0.0291
30	2.694	0.0255	0.0175	6.516	0.1166	0.9846	0.4824	0.0309	0.5210	0.6486	0.0263
40	2.971	0.0329	0.0183	5.544	0.1126	1.0360	0.5036	0.0261	0.5995	0.6443	0.0226
50	4.527	0.2602	0.2028	4.647	0.0281	0.9599	0.5208	0.0209	0.6166	0.6339	0.0183
60	5.795	0.6589	0.2502	4.378	0.0265	0.7832	0.5324	0.0152	0.5639	0.6144	0.0134
70	7.240	0.7457	0.1909	3.028	0.0185	0.5390	0.5383	0.0090	0.4366	0.5898	0.0080
80	8.616	0.7218	0.1365	1.481	0.0089	0.2631	0.5418	0.0024	0.2387	0.5641	0.0019
90	3.634	0.7624	0.0424	3.896	0.0262	—	—	—	—	—	—

$E[R_{RUP}|R_{JB}, M, \delta]$ is the mean rupture distance (R_{RUP}) for a given Joyner–Boore distance (R_{JB}), magnitude (M), and dip angle (δ). Azimuth angle (θ) and hypocenter location are randomized.

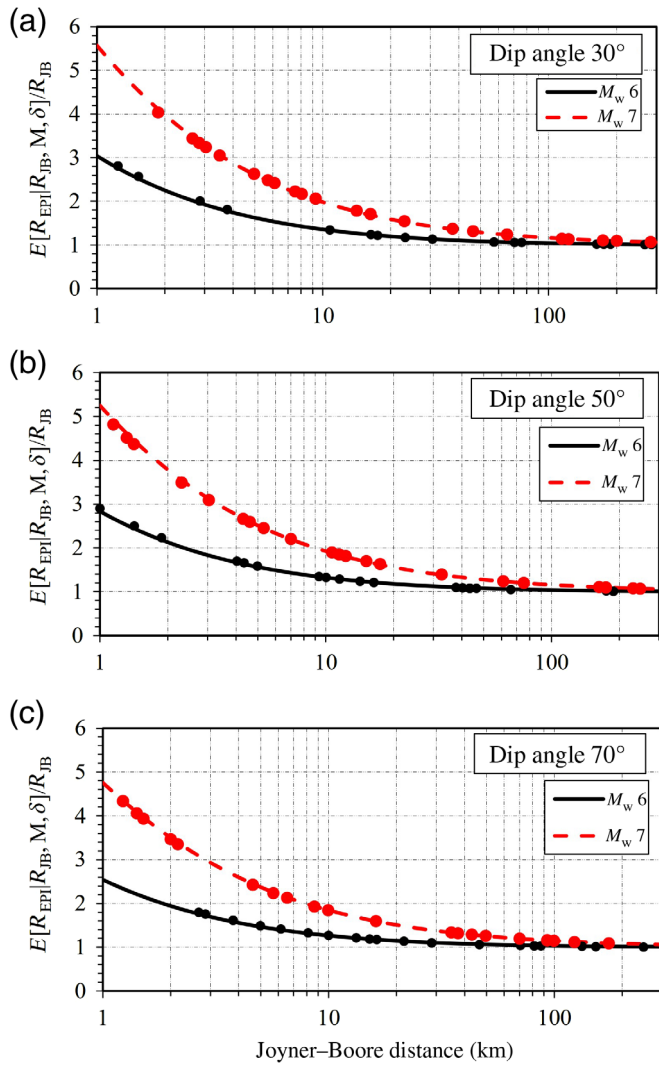


Figure 6. Comparison of the ratio of R_{EPI} to R_{JB} versus R_{JB} for dip-slip fault with dip angles of (a) 30°, (b) 50°, and (c) 70° for moment magnitudes of 6 (solid line) and 7 (dashed line). The dots represent the mean values for the distribution and the lines represent the empirical equations fitted to the distribution. The color version of this figure is available only in the electronic edition.

Similarly, for the vertical strike-slip fault ($\delta = 90^\circ$):

$$E[R_{EPI}|R_{JB}, M, \delta] = R_{JB} + C_1 \exp(C_2(M - 5))(R_{JB}^{C_3} - C_4) + C_5 R_{JB}^{C_6} + C_7 \exp(C_8(M - 5)) + \sigma_{EPI}, \quad (9)$$

in which the coefficients C_1 to C_8 are obtained from regression analysis and presented in Table 3. σ_{EPI} is the standard deviation discussed later. The coefficients are different for different dip angles. The coefficients for the dip angle not listed can be determined using interpolation. The equations are valid only when $R_{JB} \sim 0$. When $R_{JB} = 0$, the mean R_{EPI} is also zero. Figure 6 shows the variation of R_{EPI} obtained from the empirical equations (equation 8) with the mean for a dip-slip fault with dip angles of 30°, 50°, and 70°, respectively. R_{EPI} is always greater than or equal to R_{JB} at all magnitudes and dip angles. The difference between the two distances is substantial for dip-slip faults at higher magnitudes. At R_{JB} of 1 km, R_{EPI} is three times greater for $M_w 6$ and five times greater for $M_w 7$ for a 30° dip-slip fault. Because the rupture area increases with magnitude, the length and width of the fault are large for higher magnitudes, resulting in higher mean R_{EPI} values for the same R_{JB} values. This effect of large magnitude is less prominent for the vertical strike-slip fault because only one fault dimension, the length of the fault, affects R_{EPI} .

Joyner–Boore distance and hypocentral distance

Because of symmetry, the azimuth angles from 0° to 90° are used to obtain R_{HYP} for a given R_{JB} distance at the fault's different magnitude and dip angle. As discussed, separate regressions are carried out at different dip angles. Equation (10) provides the equation for the dip-slip fault and equation (11) for the vertical strike-slip fault:

$$E[R_{HYP}|R_{JB}, M, \delta, Z_{TOR}] = \sqrt{R_{JB}^2 + Z_{TOR}^2} + C_1 \exp(C_2(M - 5)^2) \times (R_{JB}^{C_3} - C_4) + C_5 R_{JB}^{C_6} + C_7 \exp(C_8(M - 5)) + \sigma_{HYP}, \quad (10)$$

TABLE 3

Coefficients for $E[R_{EPI}|R_{JB}, M, \delta]$ at Different Dip Angles (δ) for a Given Magnitude (M) and Joyner–Boore Distance (R_{JB})

δ	C_1	C_2	C_3	C_4	C_5	C_6	C_7	C_8
10	3.595	0.2506	0.24	0.8218	-0.9044	0.4764	1.267	0.5607
20	3.56	0.252	0.239	0.8151	-0.9039	0.4742	1.234	0.5588
30	3.52	0.2542	0.237	0.8044	-0.9142	0.4688	1.192	0.5495
40	3.46	0.2568	0.2345	0.7781	-0.9315	0.4609	1.107	0.5342
50	3.403	0.2601	0.2308	0.7478	-0.9674	0.443	1.023	0.5021
60	3.377	0.2637	0.2253	0.713	-1.038	0.4296	0.947	0.4405
70	3.537	0.2653	0.2151	0.6761	-1.319	0.3846	1.064	0.2525
80	3.846	0.2646	0.2021	0.6551	-1.854	0.3269	1.483	0.0026
90	0.2211	1.74	0.188	0.7227	-0.00295	1.169	0.5337	0.4944

$E[R_{EPI}|R_{JB}, M, \delta]$ is the mean epicentral distance (R_{EPI}) for a given Joyner–Boore distance (R_{JB}), magnitude (M), and dip angle (δ). Azimuth angle (θ) and hypocenter location are randomized.

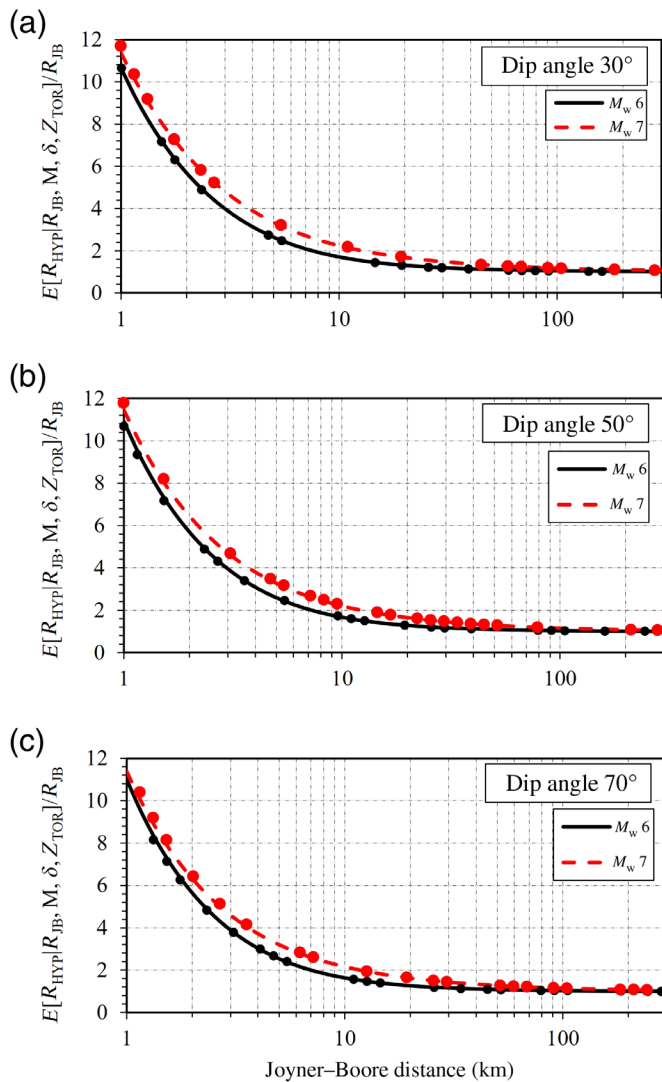


Figure 7. Comparison of the ratio of R_{HYP} to R_{JB} versus R_{JB} for dip-slip fault with dip angles of (a) 30°, (b) 50°, and (c) 70° for moment magnitudes of 6 (solid line) and 7 (dashed line). The dots represent the mean values for the distribution and the lines represent the empirical equations fitted to the distribution. The color version of this figure is available only in the electronic edition.

TABLE 4

Coefficients for $E[R_{\text{HYP}}|R_{\text{JB}}, M, \delta, Z_{\text{TOR}}]$ at Different Dip Angles (δ) for a Given Magnitude (M), Depth to the Top of the Rupture (Z_{TOR}), and Joyner-Boore Distance (R_{JB})

δ	C_1	C_2	C_3	C_4	C_5	C_6	C_7	C_8
10	4.75	0.242	0.2242	0.9981	-0.563	0.579	0.6626	0.7618
20	4.207	0.2556	0.2203	1.045	-0.5616	0.5622	1.25	0.6849
30	3.656	0.2706	0.2174	1.082	-0.608	0.5306	1.793	0.6471
40	3.112	0.2864	0.2162	1.099	-0.7109	0.4867	2.273	0.6175
50	2.634	0.3028	0.2157	1.101	-0.8945	0.4333	2.746	0.584
60	2.246	0.319	0.215	1.092	-1.135	0.3839	3.184	0.5505
70	2.02	0.3321	0.2119	1.065	-1.438	0.3429	3.601	0.511
80	1.87	0.3429	0.2075	1.041	-1.628	0.3243	3.828	0.4867
90	0.05753	2.328	0.1554	1.149	-0.3696	0.3681	2.449	0.6935

$E[R_{\text{HYP}}|R_{\text{JB}}, M, \delta, Z_{\text{TOR}}]$ is the mean hypocentral distance (R_{HYP}) for a given Joyner-Boore distance (R_{JB}), magnitude (M), dip angle (δ), and depth to top of the rupture (Z_{TOR}). Azimuth angle (θ) and hypocenter location are randomized.

$$E[R_{\text{HYP}}|R_{\text{JB}}, M, \delta, Z_{\text{TOR}}] = \sqrt{R_{\text{JB}}^2 + Z_{\text{TOR}}^2} + C_1 \exp(C_2(M-5)) \times (R_{\text{JB}}^{C_3} - C_4) + C_5 R_{\text{JB}}^{C_6} + C_7 \exp(C_8(M-5)) + \sigma_{\text{HYP}}, \quad (11)$$

in which parameters C_1 to C_8 are regression coefficients and are provided in Table 4. “ M ” is the moment magnitude, δ is the dip angle, and Z_{TOR} is the depth to the top of the rupture. σ_{HYP} is the standard deviation discussed later. The equations are valid only when $R_{\text{JB}} \sim 0$. When $R_{\text{JB}} = 0$, the mean R_{HYP} is equal to Z_{TOR} .

Apart from magnitude, dip angle, and R_{JB} distance, R_{HYP} also depends on the depth to the top of the rupture (Z_{TOR}). A comparison of the fitting of the mean values with the empirical equation (equation 10) is shown in Figure 7 for dip angles of 30°, 50°, and 70°, respectively. R_{HYP} increases slightly with increasing magnitude at small distances and converges at large R_{JB} distances.

SIGMA MODEL FOR DISTANCE METRICS CONVERSIONS

Rupture distance and Joyner-Boore distance

The sigma for R_{RUP} is based on M , δ , and R_{JB} and can be represented as follows:

$$\sigma[R_{\text{RUP}}|R_{\text{JB}}, M, \delta] = C_1 \exp(C_2(M-5)) \times \exp(-C_3 R_{\text{JB}}), \quad (12)$$

in which regression coefficients C_1 to C_3 are provided in Table 5. The coefficients are different for the mean, the hanging-wall side, or the footwall side of the fault (for vertical strike-slip fault, only coefficients for the mean are provided, as there is no hanging-wall effect). They are also different for various dip angles. As discussed previously, the coefficients for dip angles not listed can be determined by interpolation. The sigma values increase with increasing dip angles for smaller magnitudes ($M_w < 6.0$). Above M_w 6.0, no specific trends between the sigma and dip angle could be observed. The sigma also increases with increasing magnitudes for all dip angles. However, there is a decrease in sigma with increasing distance because there is less variation

TABLE 5

Coefficients for Calculation of $\sigma_{[RRUP|R_{JB},M,\delta]}$ at Different Dip Angles (δ) for a Given Magnitude (M) and Joyner–Boore Distance (R_{JB})

Dip	Mean			Footwall			Hanging Wall		
	C_1	C_2	C_3	C_1	C_2	C_3	C_1	C_2	C_3
10	0.1807	0.4005	0.0385	0.2132	0.3418	0.04356	0.1886	0.3921	0.03496
20	0.346	0.4005	0.03749	0.4249	0.3353	0.04934	0.353	0.3982	0.03056
30	0.4837	0.3958	0.03597	0.6296	0.3264	0.05632	0.4771	0.3994	0.02592
40	0.591	0.3816	0.03438	0.8203	0.3138	0.06418	0.5559	0.3908	0.02145
50	0.6763	0.3507	0.0333	0.9861	0.295	0.07151	0.5961	0.3655	0.01749
60	0.7653	0.2982	0.03472	1.114	0.2704	0.07638	0.6219	0.3137	0.01495
70	0.9143	0.2416	0.04623	1.201	0.2477	0.07897	0.698	0.2435	0.01845
80	1.124	0.213	0.06916	1.251	0.2321	0.08013	0.9934	0.1898	0.05233
90	1.091	0.3018	0.07638	–	–	–	–	–	–

Azimuth angle (θ) and hypocenter location are randomized.

TABLE 6

Coefficients for Calculation of $\sigma_{[R_{EPI}|R_{JB},M,\delta]}$ at Different Dip Angles (δ) for a Given Magnitude (M) and Joyner–Boore Distance (R_{JB})

δ	C_1	C_2	C_3	C_4	C_5	C_6
10	0.07256	1.71	0.3498	0.5909	0.7239	–0.2208
20	0.07344	1.708	0.3493	0.5906	0.7198	–0.2371
30	0.07504	1.704	0.3483	0.5921	0.7148	–0.2657
40	0.07752	1.697	0.3467	0.5918	0.7103	–0.3078
50	0.08021	1.691	0.3451	0.5899	0.7049	–0.3563
60	0.08405	1.683	0.343	0.5895	0.7101	–0.4151
70	0.09132	1.668	0.3392	0.5999	0.7467	–0.4853
80	0.1031	1.646	0.332	0.6298	0.8473	–0.5442
90	0.1678	1.848	0.1752	0.9409	1.494	–0.4161

Azimuth angle (θ) and hypocenter location are randomized.

in values at larger distances (because R_{JB} and R_{RUP} are almost the same at large distances).

Epicentral distance and Joyner–Boore distance

The standard deviation for R_{EPI} at a given R_{JB} , M, and δ for dip-slip fault can be determined using the equation:

$$\sigma_{[R_{EPI}|R_{JB},M,\delta]} = C_1 \exp(C_2(M-5))(R_{JB}^{C_3} - C_4) + C_5 R_{JB}^{C_6}. \quad (13)$$

The coefficients C_1 to C_6 are determined using regression and listed in Table 6. The coefficients are different for different dip angles. The sigma value increases with increasing magnitude and distance. Though sigma increases with dip angles at a smaller magnitude and R_{JB} , at large magnitudes, there is no significant variation in sigma values for different dip angles.

Hypocentral distance and Joyner–Boore distance

The standard deviation for R_{HYP} at a given R_{JB} , M, and δ for dip-slip fault can be determined using the following equation:

$$\sigma_{[R_{HYP}|R_{JB},M,\delta]} = C_1 \exp(C_2(M-5))(R_{JB}^{C_3} - C_4) + C_5 R_{JB}^{C_6} + C_7 \exp(C_8(M-5)). \quad (14)$$

Similarly, for the vertical strike-slip fault ($\delta = 90^\circ$):

$$\sigma_{[R_{HYP}|R_{JB},M,\delta]} = C_1 \exp(C_2(M-5)^2)(R_{JB}^{C_3} - C_4) + C_5 R_{JB}^{C_6} + C_7 \exp(C_8(M-5)). \quad (15)$$

The coefficients C_1 to C_8 are determined using regression and listed in Table 7. The coefficients differ for different dip angles, and the sigma value increases with magnitude, dip angle, and distance. For large magnitudes ($M_w > 7.5$), there is no considerable variation in sigma values for different dip angles.

APPLICATION IN GMMs

In performing PSHA, one must consider whether the source modeling approach is consistent with the distance metric used in GMMs and can be included in PSHA by calculating an additional variability due to the conversion from R_{JB} to other

TABLE 7

Coefficients for Calculation of $\sigma_{[R_{HYP}|R_{JB},M,\delta,Z_{TOR}]}$ at Different Dip Angles (δ) for a Given Magnitude (M), Depth to the Top of the Rupture (Z_{TOR}), and Joyner–Boore Distance (R_{JB})

δ	C_1	C_2	C_3	C_4	C_5	C_6	C_7	C_8
10	0.06713	1.735	0.3506	0.5713	0.4025	−0.3045	0	0
20	0.06924	1.737	0.346	0.6179	0.9081	−0.4381	0	0
30	0.07177	1.737	0.3418	0.6587	1.456	−0.4835	0	0
40	0.03256	1.897	0.4069	0.9976	−0.05961	0.7247	0.7838	0.6469
50	0.03361	1.897	0.4038	1.006	−0.2863	0.4537	1.32	0.4966
60	0.03339	1.904	0.4048	1.063	−0.4847	0.3859	1.72	0.4531
70	0.03449	1.898	0.4062	1.133	−0.5475	0.3862	1.903	0.4562
80	0.03582	1.89	0.408	1.242	−0.4631	0.4328	1.848	0.505
90	0.7622	0.3002	0.405	1.168	−0.9389	0.4699	2.303	0.4218

Azimuth angle (θ) and hypocenter location are randomized.

TABLE 8

Distance Conversion Assumptions from Different Published Studies Used for Comparison in This Study

Description	Fault Type	Magnitude-Scaling Relation	Aspect Ratio (AR)	Depth (km)
This study	Strike-slip	Somerville (2014)	1	0–15
This study	Dip-slip	Somerville (2014)	1	0–15
EPRI (2004)	Strike-slip	Somerville (2014)	3	0–25
EPRI (2004)	Dip-slip	Somerville (2014)	2	0–25
Scherbaum <i>et al.</i> (2004)	Strike-slip, dip-slip	Wells and Coppersmith (1994)	—	—
Thompson and Worden (2018)	Strike-slip	Somerville (2014)	1	0–15
Thompson and Worden (2018)	Dip-slip	Somerville (2014)	1	0–15

distance metrics. The total sigma can be calculated using the law of propagation of error as follows:

$$\sigma_{\text{total}} = \sqrt{\sigma_{\text{GMM}}^2 + \Delta\sigma^2},$$

$$\Delta\sigma^2 = \left(\frac{\partial \ln(Y)}{\partial R_{\text{GMM}}}\right)^2 \sigma_{[R_{\text{GMM}}|R_{\text{PSHA}},M,\delta]}^2, \quad (16)$$

in which σ_{GMM} is the standard deviation for the GMM, $\ln(Y)$ is the natural logarithm of the ground motion, and $\sigma_{[R_{\text{GMM}}|R_{\text{PSHA}},M,\delta]}$ is the standard deviation for the conversion from GMM distances to PSHA distances. The GMMs can be based on R_{JB} or R_{RUP} . If the GMM is based on R_{JB} and PSHA is based on R_{EPI} , then

$$\Delta\sigma^2 = \Delta\sigma_{[R_{\text{JB}}|R_{\text{EPI}},M,\delta]}^2 = \left(\frac{\partial \ln(Y)}{\partial R_{\text{JB}}}\right)^2 \sigma_{[R_{\text{JB}}|R_{\text{EPI}},M,\delta]}^2, \quad (17)$$

$$\sigma_{[R_{\text{JB}}|R_{\text{EPI}},M,\delta]}^2 = \left[\frac{\partial R_{\text{JB}}}{\partial R_{\text{EPI}}}\right]^2 \sigma_{[R_{\text{EPI}}|R_{\text{JB}},M,\delta]}^2. \quad (18)$$

We can directly calculate the $\frac{\partial R_{\text{JB}}}{\partial R_{\text{EPI}}} = \frac{1}{\left(\frac{\partial R_{\text{EPI}}}{\partial R_{\text{JB}}}\right)}$ (using the empirical equation for R_{EPI} ; $\frac{\partial R_{\text{EPI}}}{\partial R_{\text{JB}}} \neq 0$), or we can use the Taylor series expansion. If we use the Taylor series, we can consider only the first-order approximation of the second moment obtained from the Taylor expansion for simplicity. If there is no

empirical relation between the distance metrics, we can use the following approximation:

$$\frac{\partial R_{\text{JB}}}{\partial R_{\text{EPI}}} = \frac{2\Delta R_{\text{JB}}}{\langle R_{\text{EPI}} \rangle_{R_{\text{JB}}+\Delta R_{\text{JB}}} - \langle R_{\text{EPI}} \rangle_{R_{\text{JB}}-\Delta R_{\text{JB}}}}, \quad (19)$$

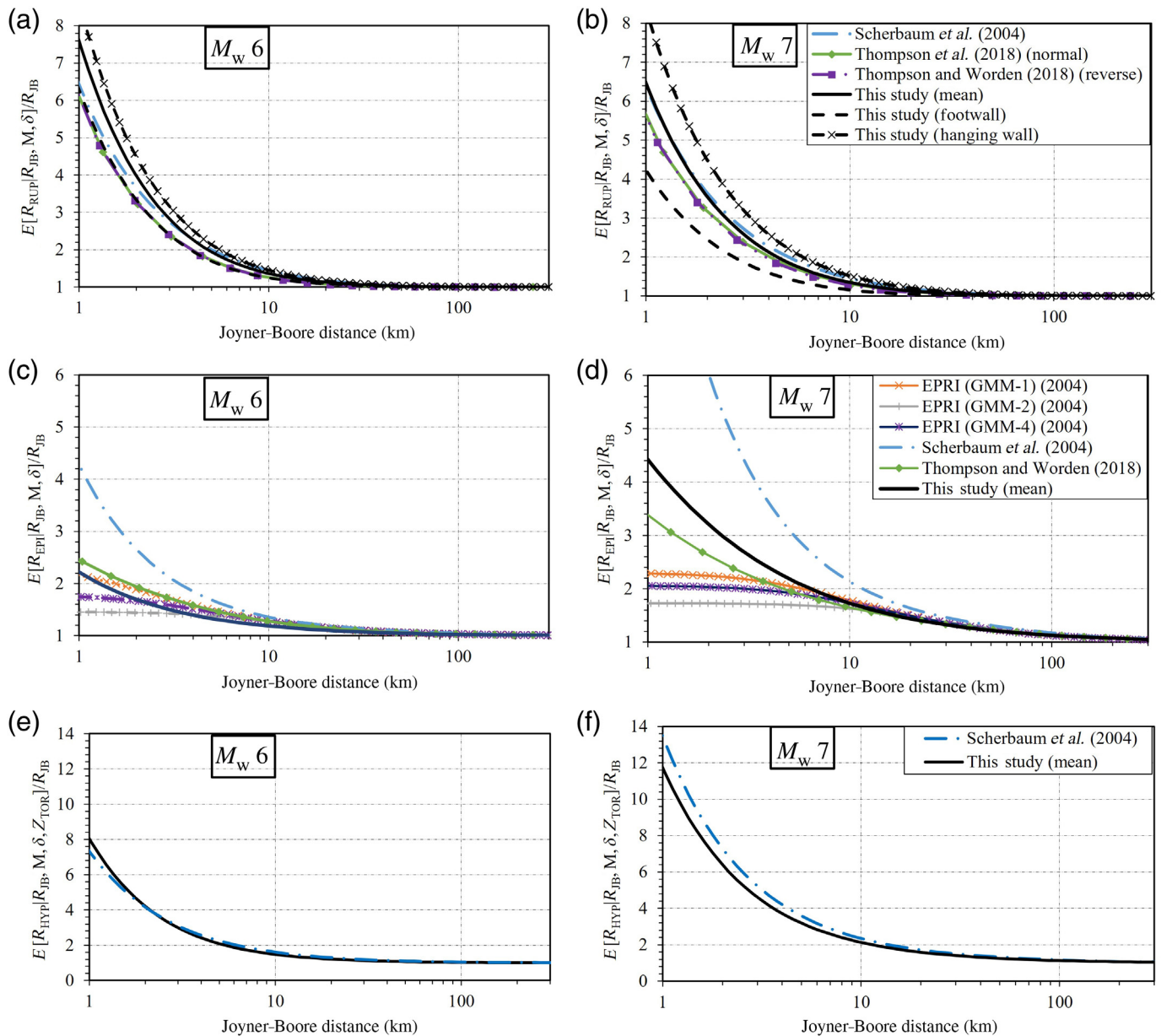
in which $\langle R_{\text{EPI}} \rangle_{R_{\text{JB}}+\Delta R_{\text{JB}}}$ is the mean R_{EPI} distance for a given reference distance of $R_{\text{JB}} + \Delta R_{\text{JB}}$. Because we have the relation between different distance metrics in our case, we can directly calculate $\frac{\partial R_{\text{JB}}}{\partial R_{\text{EPI}}}$, and $\sigma_{[R_{\text{EPI}}|R_{\text{JB}},M,\delta]}^2$ can be calculated using equation (13) for different magnitudes and dip angles. Similarly, for GMM based on R_{RUP} and PSHA based on R_{EPI} :

$$\Delta\sigma^2 = \Delta\sigma_{[R_{\text{RUP}}|R_{\text{EPI}},M,\delta]}^2 = \left(\frac{\partial \ln(Y)}{\partial R_{\text{RUP}}}\right)^2 \sigma_{[R_{\text{RUP}}|R_{\text{EPI}},M,\delta]}^2. \quad (20)$$

We can also calculate similar values for R_{HYP} and R_{RUP} using equations (14 and 15) and equation (12), respectively.

COMPARISON WITH OTHER MODELS

We compared our results with the equations provided by Scherbaum *et al.* (2004), EPRI (2004), and Thompson and Worden (2018). Scherbaum *et al.* (2004) provided a polynomial equation with different coefficients for different distance conversions. Different GMMs have been defined by EPRI (2004): three



models (GMM-1, GMM-2, and GMM-4) based on R_{JB} distance, and one model (GMM-3) based on R_{RUP} distance. They have also provided equations to convert these distance metrics to R_{EPI} distance for each GMM. The assumptions for each published study we have used for comparison are listed in Table 8. Figure 8 shows the variation of the ratio of R_{target} to R_{JB} versus R_{JB} for different magnitude events and compares the values with those obtained from other published studies. Because Scherbaum *et al.* (2004) is limited to M_w 7.5, we have provided a comparison for M_w 6 and 7. For the ratio of R_{EPI} to R_{JB} , Scherbaum *et al.* (2004) predict higher values at smaller distances (<10 km), whereas EPRI predicts comparatively lower values. The values for the strike-slip model developed in this study closely follow other studies for distances greater than 10 km at all magnitudes. The values obtained from the proposed empirical equations and Thompson and Worden (2018) differ from EPRI (2004) at smaller distances

Figure 8. Comparison with other models for mean distance conversion at (a,c,e) magnitude 6 and (b,d,f) magnitude 7 for R_{RUP} , R_{EPI} , and R_{HYP} . The mean results for R_{EPI} and R_{HYP} are based on the strike-slip fault, and the mean results for R_{RUP} are based on the 60° dip-slip fault. The comparison is made with other published studies that provide a relationship for the conversion of each distance metric. For example, Scherbaum *et al.* (2004) provide relationships for R_{JB} , R_{RUP} , R_{EPI} , and R_{HYP} , whereas EPRI (2004) and Thompson and Worden (2018) provide relationships only for R_{EPI} , R_{JB} , and R_{RUP} . For R_{HYP} , the Z_{TOR} value is fixed at 3 km. The color version of this figure is available only in the electronic edition.

(<10 km) for M_w 7. The differences in values result from different assumptions and methodologies. The calculations used in this study and Thompson and Worden (2018) are also independent of GMMs or the oscillator period. Overall, the values are consistent with the other published studies.

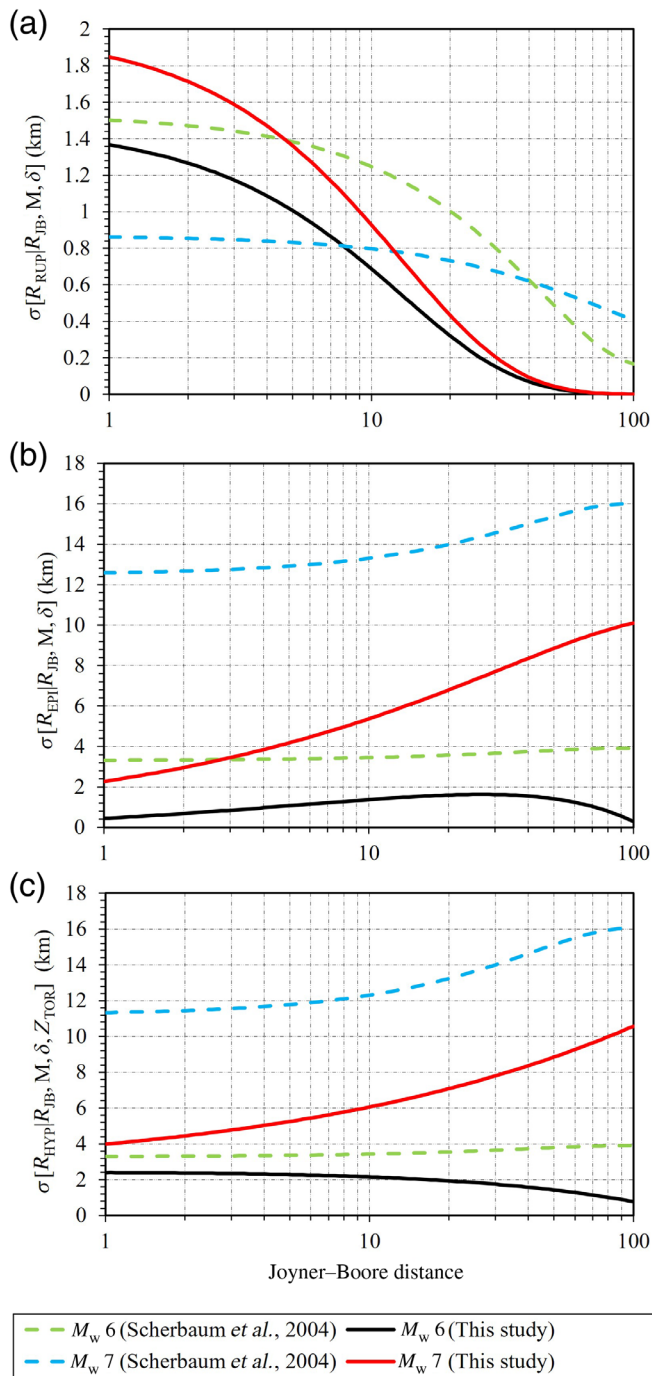


Figure 9. Compares the standard deviation for (a) R_{RUP} , (b) R_{EPI} , and (c) R_{HYP} versus R_{JB} obtained from this study and Scherbaum et al. (2004) for vertical strike-slip fault for magnitude 6 and 7. The color version of this figure is available only in the electronic edition.

The comparison of variation of the ratio of R_{RUP} to R_{JB} versus R_{JB} is also presented in Figure 8 for M_w 6 and 7. The comparison is shown for the dip-slip fault. For the comparison, we have used a dip angle of 60°, though other dip angles also provide similar results. EPRI (2004) does not provide a separate equation to convert between R_{JB} and R_{RUP} . The values obtained from this study are slightly higher at a smaller distance

(<10 km) compared to other published studies for M_w 6. The values are consistent at distances greater than 10 km for all magnitudes. The variation in the values at distances less than 10 km is the direct result of the choice of depth to the top of the rupture (Z_{TOR}). At smaller distances, the calculated R_{RUP} is directly affected by Z_{TOR} . Z_{TOR} does not have a significant impact on R_{RUP} at large distances. For magnitude 7, the mean R_{RUP} distance calculated in this study is similar to other published studies. For all magnitudes, the calculated R_{RUP} distance from all the studies falls between the R_{RUP} distance calculated for the hanging wall and the footwall in this study.

Only Scherbaum et al. (2004) have provided an empirical relationship between R_{HYP} and R_{JB} . The values are consistent with this study for M 6 and 7. For calculation, we have assumed the depth to the top of the rupture as 3 km. Similar to R_{RUP} , R_{HYP} is also sensitive to Z_{TOR} value at small distances.

The sigma of the proposed model in this study is considerably smaller than Scherbaum et al. (2004), as shown in Figure 9 for R_{RUP} , R_{EPI} , and R_{HYP} . The sigma obtained from Scherbaum et al. (2004) for R_{EPI} is much larger for all magnitudes, and similar trends can be observed for R_{HYP} . For R_{RUP} , at smaller distances (<10 km for M 6), the sigma values are slightly higher for this study compared to Scherbaum et al. (2004). However, the difference is negligible (<0.5 km). The sigma has not been compared with EPRI as it depends on GMMs, so a comparison would not be valid. Similarly, Thompson and Worden (2018) use R_{EPI} as reference distance, so a direct comparison of sigma is not possible.

IMPLICATIONS FOR THE PSHA

In PSHA, the integral over various seismic sources, such as faults and areal sources, is conducted for each site for different magnitudes and distances. Areal sources are assigned when we do not have enough information about the fault, such as in some CEUS regions. They are generally used for low and moderate seismicity. The areal source is subdivided into grids in which each grid acts as a point source. The distance from each point source to the site can be described using point-based distances such as R_{EPI} or R_{HYP} . Because we do not have enough information about the fault in such cases, it is challenging to use fault-based distances such as R_{JB} and R_{RUP} .

The total variation in the calculated seismic hazard due to the conversion of distance and their associated uncertainties can be demonstrated by considering a simple seismic source. We have considered a circular seismic source with a radius of 100 km. The seismicity of the source follows a truncated exponential model with $\lambda(M \geq 5) = 0.0395$ and b -value of 0.9. The magnitude is truncated from 5.0 to 7.5. We have conducted PSHA calculations using the Pezeshk et al. (2011) GMM based on R_{RUP} distance. The seismic source is divided into grids, in which each grid acts like a point source. A site is assumed at the center of the areal seismic source. We calculate the epicentral distance by measuring the distance from each point source to

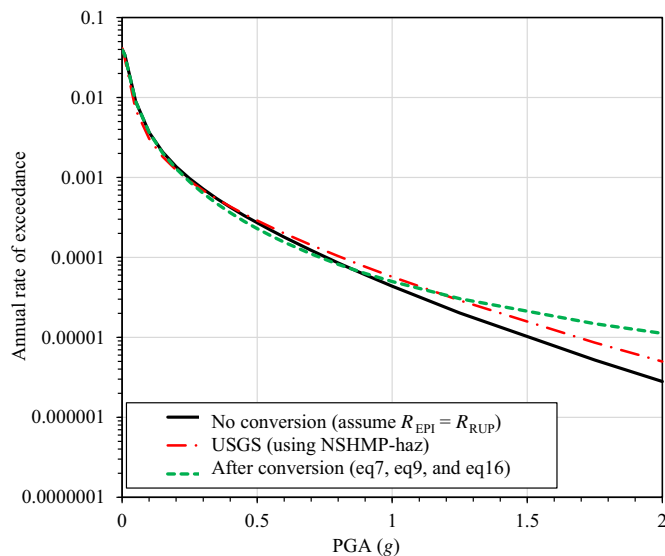


Figure 10. Annual hazard curves for a circular seismic source with a radius of 100 km based on R_{RUP} -based ground-motion model (GMM; [Pezeshk et al., 2011](#)) using distance conversion equations developed in this study. Annual hazard curves without distance conversion and those based on U.S. Geological Survey (USGS) National Seismic Hazard Mapping Project (NSHMP-haz) are also shown for reference. The color version of this figure is available only in the electronic edition.

the site. However, the GMM is based on R_{RUP} distance. Hence, for consistency between PSHA and GMM, we need to convert the distances.

At a sample R_{EPI} distance of 30 km for a vertical strike-slip fault of magnitude 7.0, we obtain a R_{JB} distance of 21.1 km and an R_{RUP} distance of 23.4 km. So, for a 30 km R_{EPI} distance used in PSHA for an areal source, we need to use an R_{RUP} distance of 23.4 km in the GMM for consistency. Because the equivalent R_{RUP} distance is smaller than the R_{EPI} distance in this example, it increases the calculated seismic hazard. In this example, there is no direct way to convert from R_{EPI} to R_{JB} because the equations developed in this study are based on R_{JB} . So, we determine R_{EPI} values for different R_{JB} values for a given magnitude using equation (9) and populate a table. We can use this table to determine R_{JB} values for the required R_{EPI} values. Then, we can use the R_{JB} value to determine R_{RUP} distance for a given magnitude and dip angle using equation (7). The additional sigma due to distance conversion must also be included in the PSHA to obtain accurate seismic hazard results. The equation for the derivative of GMM, which is necessary to determine the total sigma, is provided in the supplemental material. Based on the mean and the total sigma, we determine the mean exceedance at different magnitudes and distances to calculate the seismic hazard. Figure 10 shows the mean annual exceedance of hazard based on [Pezeshk et al. \(2011\)](#) using the proposed empirical equations. The solid black lines represent the hazard without any distance conversion. Below the peak ground acceleration (PGA) of 1.0g, the values are comparable

to results from USGS National Seismic Hazard Mapping Project, NSHMP-haz, code for a similar seismic source (shown with dotted-dashed red lines). The values are slightly higher above the PGA of 1.0g. The green dashed lines show the result after appropriate conversion and using total sigma, considering the effects of distance conversion on estimating sigma using equation (16). We can observe a significant variation in the hazard estimation when we convert the distances for this study above a PGA of 1.0g. Hence, one must convert to appropriate distances and project their uncertainties in the PSHA calculations to obtain accurate seismic hazards.

CONCLUSIONS

This study provides empirical relations among different distance metrics. The equations were developed with an emphasis on stable continental regions. As a result, we have used [Somerville \(2014\)](#) to describe the relationship between the rupture area and the magnitude of the earthquake. We have demonstrated that R_{JB} can be effectively used to determine other source-to-site distance metrics based on the property of the fault. We determine the difference between the various distance metrics and R_{JB} . These differences can be described using a gamma distribution. The functional forms for R_{target} are based on the magnitude and the dip angle of the fault (also Z_{TOR} for R_{HYP}) for a random azimuth and hypocenter location. Because the empirical equations provide a mean estimate of the required distance measure for a given magnitude and the dip angle of the fault, these equations may not be effective when the location of the hypocenter or the azimuth of the fault is known. A method to determine the sigma of the obtained results has also been discussed. These equations are also helpful in PSHA to reliably convert from R_{JB} to other rupture-based distances (R_{RUP}) and point-based distances (R_{EPI} and R_{HYP}). The equations for variability can be used to obtain the total sigma for use in PSHA. To use these equations, we only need basic information on the type of faulting, applicable source-scaling equations, and the dip angle of the fault based on available geologic and tectonic information. If the dip angle is unknown, we can assume a dip angle of 40° ([Kaklamanos et al., 2011](#)) and apply appropriate sigma values.

Though these distance metrics are closer to each other at large distances, there are significant differences between them at smaller distances. Ignoring these differences will result in inaccurate seismic hazard calculations closer to the fault. With interest high in developing accurate GMMs for the near-fault areas, we should also consider the effect of different distance metrics in PSHA to obtain accurate seismic hazard of the area. Unlike previous models developed by [EPRI \(2004\)](#) and [Scherbaum et al. \(2004\)](#), which are only dependent on magnitude, the proposed models also depend on the effect of the dip angle for estimating different distance measures. [Scherbaum et al. \(2004\)](#) model is also highly unstable for larger magnitudes (greater than 7.5) and distances greater than

100 km. We also consider the effect of hanging wall and foot-wall for the conversion of R_{RUP} . The empirical equations developed in this study are purely based on the geometry of the fault and are not dependent on GMMs. Hence, the equations can be applied directly in seismic hazard applications for any preferred GMMs, which avoids complex integrations involved in Thompson and Worden (2018) and Tavakoli *et al.* (2018). Using the distance conversion equations and their respective uncertainties, we can better estimate the seismic hazard for the region of interest.

DATA AND RESOURCES

Most of the analyses were performed using MATLAB R2018a release available at <https://www.mathworks.com/products/matlab.html>. Plots were made using MATLAB. The data for Thomson and Worden were available at <https://github.com/usgs/ps2ff/tree/master/ps2ff/tables>. The U.S. Geological Survey (USGS) National Seismic Hazard mapping code is available at <https://code.usgs.gov/ghsc/nshmp/nshmp-haz>. The supplemental material includes the methods to derive the equations for the distance metrics and the derivative of Pezeshk *et al.* (2011). All web-sites were last accessed in July 2022.

DECLARATION OF COMPETING INTERESTS

The authors acknowledge that there are no conflicts of interest recorded.

ACKNOWLEDGMENTS

The authors would like to thank all the anonymous reviewers for their help and input in this study.

REFERENCES

- Abrahamson, N. A., and W. J. Silva (2008). Summary of the Abrahamson & Silva NGA ground-motion relations, *Earthq. Spectra* **24**, 67–97.
- Akkar, S., M. A. Sandikkaya, and J. J. Bommer (2014). Empirical ground-motion models for point- and extended-source crustal earthquake scenarios in Europe and the Middle East, *Bull. Earthq. Eng.* **12**, no. 1, 359–387, doi: [10.1007/s10518-013-9461-4](https://doi.org/10.1007/s10518-013-9461-4).
- Bommer, J. J., and S. Akkar (2012). Consistent source-to-site distance metrics in ground-motion prediction equations and seismic source models for PSHA, *Earthq. Spectra* **28**, no. 1, 1–15, doi: [10.1193/1.3672994](https://doi.org/10.1193/1.3672994).
- Bommer, J. J., B. Dost, B. Edwards, P. J. Stafford, J. Elk, D. Doornhof, and M. Ntinalexis (2016). Developing an application-specific ground-motion model for induced seismicity, *Bull. Seismol. Soc. Am.* **106**, no. 1, 158–73, doi: [10.1785/0120150184](https://doi.org/10.1785/0120150184).
- Campbell, K. W., and Y. Bozorgnia (2014). NGA-west2 ground motion model for the average horizontal components of PGA, PGV, and 5% damped linear acceleration response spectra, *Earthq. Spectra* **30**, no. 3, 1087–1115, doi: [10.1193/062913EQS175M](https://doi.org/10.1193/062913EQS175M).
- Campbell, K. W., and N. Gupta (2018). Modeling diffuse seismicity in probabilistic seismic hazard analysis: Treatment of virtual faults, *Earthq. Spectra* **34**, no. 3, 1135–1154, doi: [10.1193/041117EQS070M](https://doi.org/10.1193/041117EQS070M).
- Chiou, B. S. J., and R. R. Youngs (2008). An NGA model for the average horizontal component of peak ground motion and response spectra, *Earthq. Spectra* **24**, 173–215.
- Electric Power Research Institute (EPRI) (2004). CEUS ground motion project final report, EPRI report, *EPRI Rept. 1009684*, December 2004, available at <https://www.nrc.gov/docs/ML0504/ML050450305.pdf> (last accessed March 2023).
- Hanks, T. C., and W. H. Bakun (2008). M-log A observations for recent large earthquakes, *Bull. Seismol. Soc. Am.* **98**, 490–494.
- Kaklamanos, J., L. G. Baise, and D. M. Boore (2011). Estimating unknown input parameters when implementing the NGA ground-motion prediction equations in engineering practice, *Earthq. Spectra* **27**, no. 4, 1219–1235, doi: [10.1193/1.3650372](https://doi.org/10.1193/1.3650372).
- Mai, P., P. Martin, P. Spudich, and J. Boatwright (2005). Hypocenter locations in finite-source rupture models, *Bull. Seismol. Soc. Am.* **95**, no. 3, 965–980, doi: [10.1785/0120040111](https://doi.org/10.1785/0120040111).
- Monelli, D., M. Pagani, G. Weatherill, L. Danciu, and J. Garcia (2014). Modeling distributed seismicity for probabilistic seismic-hazard analysis: Implementation and insights with the OpenQuake engine, *Bull. Seismol. Soc. Am.* **104**, 1636–49.
- Petersen, M. D., A. D. Frankel, S. C. Harmsen, C. S. Mueller, K. M. Haller, R. L. Wheeler, R. L. Wesson, Y. Zeng, O. S. Boyd, D. M. Perkins, *et al.* (2010). Documentation for the 2008 update of the United States National Seismic Hazard maps, *Earthquake Research: Background and Select Rept.* 107–234, doi: [10.3133/ofr20081128](https://doi.org/10.3133/ofr20081128).
- Pezeshk, S., A. Zandieh, and B. Tavakoli (2011). Hybrid empirical ground-motion prediction equations for eastern North America using NGA models and updated seismological parameters, *Bull. Seismol. Soc. Am.* **101**, no. 4, 1859–1870, doi: [10.1785/0120100144](https://doi.org/10.1785/0120100144).
- Scherbaum, F., J. Schmedes, and F. Cotton (2004). On the conversion of source-to-site distance measures for extended earthquake source models, *Bull. Seismol. Soc. Am.* **94**, no. 3, 1053–1069, doi: [10.1785/0120030055](https://doi.org/10.1785/0120030055).
- Shaw, B. E., and S. G. Wesnousky (2008). Slip-length scaling in large earthquakes: The role of deep-penetrating slip below the seismogenic layer, *Bull. Seismol. Soc. Am.* **98**, no. 4, 1633–1641.
- Somerville, P. (2014). Scaling relations between seismic moment and rupture area of earthquakes in stable continental regions, *PEER Rept.* doi: [10.1177/8755293020988024](https://doi.org/10.1177/8755293020988024).
- Somerville, P. G., N. Collins, N. A. Abrahamson, R. Graves, and C. K. Saikia (2001). Ground motion attenuation relations for the central and eastern United States, *Rept. U.S. Geol. Surv. NEHRP External Research Program, Award No. 99-HQ-GR-0098*.
- Tavakoli, B., F. Sedaghati, and S. Pezeshk (2018). An analytical effective point-source-based distance-conversion approach to mimic the effects of extended faults on seismic hazard assessment, *Bull. Seismol. Soc. Am.* **108**, no. 2, 742–760, doi: [10.1785/0120170171](https://doi.org/10.1785/0120170171).
- Thompson, E. M., and C. B. Worden (2018). Estimating rupture distances without a rupture, *Bull. Seismol. Soc. Am.* **108**, no. 1, 371–379, doi: [10.1785/0120170174](https://doi.org/10.1785/0120170174).
- Wells, D. L., and K. J. Coppersmith (1994). New empirical relationships among magnitude, rupture length, rupture width, rupture area, and surface displacement, *Bull. Seismol. Soc. Am.* **84**, no. 4, 974–1002.

Manuscript received 1 October 2022

Published online 28 March 2023